

# Tau flavored dark matter and its impact on tau Yukawa coupling

Wei Chao<sup>1,\*</sup>, Huai-Ke Guo<sup>1,†</sup> and Hao-Lin Li<sup>1‡</sup>

*Amherst Center for Fundamental Interactions, Department of Physics,*

*University of Massachusetts-Amherst Amherst, MA 01003 USA*

## Abstract

In this paper we perform a systematic study of the tau flavored dark matter model by introducing two kinds of mediators (a scalar doublet and a charged scalar singlet). The electromagnetic properties of the dark matter, as well as their implications in dark matter direct detections, are analyzed in detail. The model turns out contributing a significant radiative correction to the tau lepton mass, in addition to loosening the tension between the measured dark matter relic density and constraints of dark matter direct detections. The loop corrections can be  $\mathcal{O}(10\%)$  of the total tau mass. Signal rates of the Higgs measurements from the LHC in the  $h \rightarrow \tau\tau$  and  $h \rightarrow \gamma\gamma$  channels, relative to the Standard Model expectations, can be explained in this model.

---

\* chao@physics.umass.edu

† huaike@physics.umass.edu

‡ haolinli@physics.umass.edu

## I. INTRODUCTION

Accumulated cosmological and astrophysical observations have confirmed the existence of the cold dark matter  $\Omega h^2 = 0.1199 \pm 0.0022$  [1], which requires an extension to the minimal Standard Model (SM). Since the nature of the dark matter and the way it interacts with the SM particles remain mysteries, it catalyzes various portals of the dark matter. Strengths of interactions between ordinary matter and dark matter are severely constrained by the observed dark matter relic abundance and exclusion limits from dark matter direct and indirect detections. Thanks to the advancement of the technology, many well-motivated dark matter models were tested and excluded by the dark matter direct and(or) indirect detection experiments! It raises challenge to the dark matter model building, but shows people hope of discovering dark matter in the laboratory.

Among various dark matter models, flavored dark matter [3–26] is interesting and appealing for the following three reasons: (1) It may naturally explain the galactic center gamma ray excess [17] observed by the *Fermi-LAT* [27]. (2) It is tightly connected with the flavor physics. (3) It may release the tension between the observed dark matter relic density and constraints from underground laboratory direct detections. Besides, collider searches of the flavored dark matters are accessible and it was pointed out that collider searches are remarkably complementary for the quark(lepton)-portal dark matter models [21–25]. Notice that dark matter could be incorporated into numerous models of flavors. It deserves a systematic study of these models.

In this paper we study phenomenologies of the tau lepton flavored dark matter by assuming dark matter is a Dirac fermion and mainly couples to the third generation leptons with an extra scalar doublet and a charged scalar singlet as mediators. We focus on the following aspects of this model: i) the dark matter electromagnetic form factors, ii) its relic density, iii) signatures in the dark matter direct detection and iv) the impact of the model to the  $h\bar{\tau}\tau$  coupling as well as  $h\gamma\gamma$  coupling, where  $h$  is the SM-like Higgs. Our findings can be summarized as the followings:

- The tension between the dark matter relic density and direct detection is highly loosed even for  $\mathcal{O}(1)$  Yukawa couplings of the dark matter with tau lepton. The charge radius of the dark matter dominates the scattering of the dark matter with the nuclei for light dark matter case while the magnetic moment plays more important role in direct

detections for the heavy dark matter case.

- The Yukawa coupling of  $h\bar{\tau}\tau$  can be significantly changed compared to the SM case. Tau lepton mass arises from two parts in this model: the general Yukawa interaction and the one-loop radiative correction, whose effect is roughly proportional to the dark matter mass. It turns out the loop effect can contribute about  $\mathcal{O}(10\%)$  of the total tau mass.
- Higgs to diphoton decay rate can be slightly modified in this model. The ratio  $\mu_{\gamma\gamma}$  can be in the range (0.7, 1.25), which is still consistent the current bounds given by the ATLAS and CMS collaborations.

The signatures of the dark matter at colliders are also briefly discussed in the paper. Compared with previous studies of lepton portal dark matter models , as was mentioned in the references, our studies are new in the following aspects: (1) We focus on the multi-mediator scenario; (2) The Yukawa couplings of  $h\bar{\tau}\tau$  and  $h\gamma\gamma$  can be significantly modified in this model.

Let's comment on a possible extension of this tau flavored dark matter model. If one assumes the dark matter couples both to the muon and tau leptons, then the observed Higgs to  $\tau\mu$  decay rate [28, 29] can be generated, but it also gives an overly estimated branching ratio of  $\tau \rightarrow \mu\gamma$ . Thus the lepton flavored dark matter model can hardly explain the Higgs lepton-flavor-violating decays.

The remaining of this paper is organized as follows: We briefly describe our model in section II. Section III is focused on the phenomenologies of the model, including dark matter relic density, signatures in direct detections, the  $\tau$ -lepton mass,  $h \rightarrow \bar{\tau}\tau$  and  $h \rightarrow \gamma\gamma$  decay rate. The last part is concluding remarks.

## II. MODEL

We extend the SM with an inert scalar doublet, a singly charged scalar singlet and a Dirac dark matter, which is stabilized by a  $Z_2$  discrete flavor symmetry, under which dark matter and the third generation leptons are odd while all other particles are even. In the following we first describe scalar interactions, then go to the dark matter interactions. The

scalar potential can be written as

$$\begin{aligned}
V = & -\mu^2 H^\dagger H + \lambda(H^\dagger H)^2 + m_1^2 \Phi^\dagger \Phi + \lambda_1(\Phi^\dagger \Phi)^2 + \lambda_2(\Phi^\dagger \Phi)(H^\dagger H) + \lambda_3(\Phi^\dagger H)(H^\dagger \Phi) \\
& + m_2^2 S^+ S^- + \lambda_4(S^+ S^-)^2 + \lambda_5(S^+ S^-)(H^\dagger H) + \lambda_6(S^+ S^-)(\Phi^\dagger \Phi) \\
& + \sqrt{2}\Lambda H^T \varepsilon \Phi S^- + \text{h.c.} ,
\end{aligned} \tag{1}$$

where  $H^T \equiv (G^+, (h + iG_0 + v)/\sqrt{2})$  is the SM Higgs doublet,  $v = 246$  GeV is the vacuum expectation value (VEV),  $\Phi^T \equiv (\Phi^+, (\rho + i\eta)/\sqrt{2})$  is the inert scalar doublet,  $S^\pm$  is the singly charged scalar singlet and  $\Lambda$  has mass dimension +1. Assuming that the mass term of  $\Phi$  is positive, it develops no VEV. As a result, there is no mixing between  $h$  and  $\rho$ . The masses of neutral scalars can be written as

$$m_h^2 = 2\lambda v^2, \quad m_\rho^2 = m_\eta^2 = m_1^2 + \frac{1}{2}(\lambda_2 + \lambda_3)v^2. \tag{2}$$

Due to the last term in Eq. (1), there is mixing between  $\Phi^+$  and  $S^+$  and the relevant mass matrix is

$$\begin{pmatrix} m_1^2 + \frac{1}{2}\lambda_2 v^2 & -\Lambda v \\ -\Lambda v & m_2^2 + \frac{1}{2}\lambda_5 v^2 \end{pmatrix}. \tag{3}$$

The corresponding mass eigenvalues are

$$\hat{m}_{1,2}^2 = \frac{1}{2} \left\{ m_1^2 + m_2^2 + \frac{1}{2}(\lambda_2 + \lambda_5)v^2 \pm \sqrt{\left[ m_1^2 - m_2^2 + \frac{1}{2}(\lambda_2 - \lambda_5)v^2 \right]^2 + 4(\Lambda v)^2} \right\}, \tag{4}$$

and the relations between physical eigenstates and interaction eigenstates are  $\Phi^+ = c_\theta \hat{\Phi}^+ + s_\theta \hat{S}^+$ ,  $S^+ = -s_\theta \hat{\Phi}^+ + c_\theta \hat{S}^+$ , where  $c_\theta = \cos \theta$  and  $s_\theta = \sin \theta$ , with  $\theta$  the rotation angle that diagonalizes the mass matrix in Eq.3.

Free parameters of this model are:  $m_h$ ,  $m_\rho$ ,  $\hat{m}_{1,2}$ ,  $\theta$ ,  $\lambda_i (i = 1, 2, 4, 5, 6)$ , and  $\Lambda$ . Unphysical parameters in the Higgs potential can be written in terms of the physical parameters:

$$(A) \begin{cases} \mu^2 = 1/2 m_h^2 \\ m_1^2 = \hat{m}_1^2 c_\theta^2 + \hat{m}_2^2 s_\theta^2 - 1/2 \lambda_2 v^2 \\ m_2^2 = \hat{m}_1^2 s_\theta^2 + \hat{m}_2^2 c_\theta^2 - 1/2 \lambda_5 v^2 \end{cases} \quad (B) \begin{cases} \lambda = m_h^2 v^{-2} / 2 \\ \Lambda = (\hat{m}_1^2 - \hat{m}_2^2) c_\theta s_\theta v^{-1} \\ \lambda_3 = 2v^{-2} [m_\rho^2 - (\hat{m}_1^2 c_\theta^2 + \hat{m}_2^2 s_\theta^2)] \end{cases} \tag{5}$$

Notice that in the parameter set we have chosen,  $\lambda_1, \lambda_4, \lambda_6$  describe quartic interactions among these extra scalars and are not so relevant for the study in this paper.  $\lambda_2$  and  $\lambda_5$  are relevant for the  $h\gamma\gamma$  and  $h\bar{\tau}\tau$  couplings as will be seen in the next section.

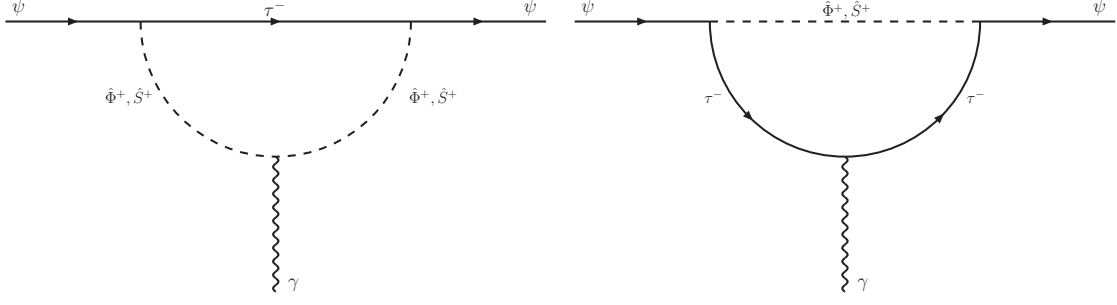


FIG. 1: Feynman diagrams contributing to the dark matter electromagnetic form factors.

We assume that dark matter only interacts with the new scalars and third generation leptons which can be written as

$$- \mathcal{L}_Y = \kappa_1 \bar{\ell}_L^3 \tilde{\Phi} \psi + \kappa_2 \bar{\psi} S^+ \tau_R + \text{h.c.} , \quad (6)$$

where  $\ell_L^3$  is the third generation left-handed lepton doublet,  $\tau_R$  is the right-handed tau lepton and  $\psi$  is the Dirac dark matter. As a result, the dark matter can only annihilate into  $\bar{\tau}\tau$  and  $\bar{\nu}_\tau\nu_\tau$ . For the benefit of the direct detection, one needs to calculate the electromagnetic form factors of the dark matter, which arise at one loop level from the relevant Feynmann diagrams shown in Fig. 1. The induced effective dark matter-photon interactions are

$$\Delta \mathcal{L}_{\text{EM}}^\psi = b_\psi \bar{\psi} \gamma^\mu \psi \partial^\nu F_{\mu\nu} + c_\psi \bar{\psi} \gamma^\mu \gamma^5 \psi \partial^\nu F_{\mu\nu} + \frac{\mu_\psi}{2} \bar{\psi} \sigma^{\mu\nu} \psi F_{\mu\nu}, \quad (7)$$

where  $b_\psi$  is the charge radius,  $c_\psi$  is the axial charge radius or anapole moment and  $\mu_\psi$  is the magnetic moment. Since there is no CP violation in the dark matter sector, the electric dipole moment term is absent. We assume the following mass hierarchy  $m_\tau \ll m_\psi < \hat{m}_{1,2}, m_{\rho,\eta}$ . Besides the typical momentum transfer of DM-Nucleon interactions is about 50 MeV, thus the momentum transfer,  $\sqrt{-q^2}$ , is far smaller than the  $\tau$  mass and constitutes the smallest scale. Collecting all the contributing diagrams and expanding in terms of  $q^2$ , we obtain

$$\begin{aligned} \mu_\psi &= \sum_{i=1}^2 -\frac{em_\psi \zeta_i}{64\pi^2} \int_0^1 dx \frac{x(1-x)}{\Delta_i}, \\ b_\psi &= \sum_{i=1}^2 \frac{e\zeta_i}{32\pi^2} \int_0^1 dx \left\{ \frac{x^3 - 2(1-x)^3}{6\Delta_i} + \frac{(x-1)^3(x^2m_\psi^2 + m_\tau^2) + 2(1-x)x^4m_\psi^2}{6\Delta_i^2} \right\}, \\ c_\psi &= \sum_{i=1}^2 \frac{e\hat{\zeta}_i}{192\pi^2} \int_0^1 dx \left\{ \frac{(-3x^3 + 6x^2 - 6x + 2)x\hat{m}_i^2 + (-2x^4 + 6x^3 - 9x^2 + 7x - 2)xm_\psi^2}{\Delta_i^2} \right\}, \end{aligned} \quad (8)$$

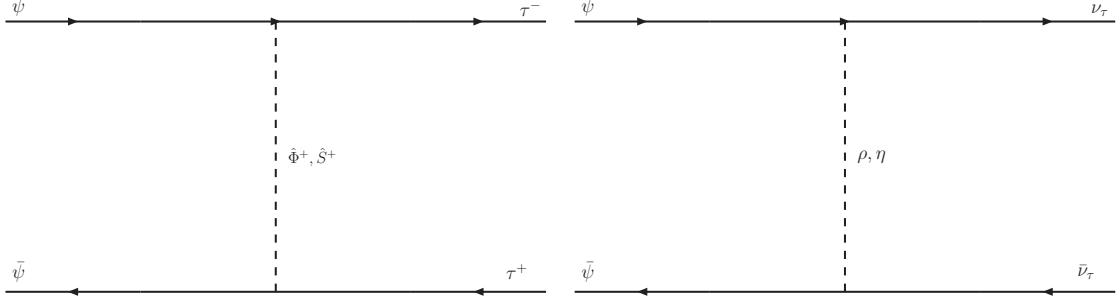


FIG. 2: Dark matter annihilation channels.

where  $m_\psi$  is the dark matter mass,  $\zeta_1 = c_\theta^2 \kappa_1^2 + s_\theta^2 \kappa_2^2$ ,  $\zeta_2 = s_\theta^2 \kappa_1^2 + c_\theta^2 \kappa_2^2$ ,  $\hat{\zeta}_1 = c_\theta^2 \kappa_1^2 - s_\theta^2 \kappa_2^2$ ,  $\hat{\zeta}_2 = s_\theta^2 \kappa_1^2 - c_\theta^2 \kappa_2^2$ , and  $\Delta_i = x \hat{m}_i^2 + x(x-1)m_\psi^2 + (1-x)m_\tau^2$ . We have ignored terms proportional to  $\mathcal{O}(m_\tau^2)$  in Eq. (8). Note that the limit  $m_\psi, m_\tau \ll \hat{m}_{1,2}$  allows us to recover the familiar result [21, 30]

$$b_\psi = \sum_i \frac{e\zeta_i^2}{64\pi^2 \hat{m}_i^2} \left( 1 + \frac{2}{3} \ln \frac{m_\tau^2}{\hat{m}_i^2} \right), \quad (9)$$

where  $m_\tau$  serves as an infrared regulator.

Similarly there are also form factors for the effective dark matter-Z boson interactions. The contribution of these interactions to the dark matter-nuclei scattering cross section is subdominant compared with those arising from electromagnetic form factors. So we neglect these interactions in our calculation.

### III. PHENOMENOLOGY

We will study in this section phenomenologies arising from this model, including the dark matter relic density, signatures in direct detections, the loop induced  $\tau$  lepton mass, the effective coupling of  $h\bar{\tau}\tau$  as well as the Higgs to diphoton decay rate. Finally we will discuss signatures of our model at colliders.

#### A. Relic density

We have assumed that the dark matter is a Dirac fermion and only interacts with the third generation leptons in our model. It annihilates into  $\bar{\tau}\tau/\bar{\nu}_\tau\nu_\tau$  with the relevant Feynman diagrams shown in Fig. 2. The cold dark matter was in local thermodynamic equilibrium in

the early Universe. When its interaction rate drops below the expansion rate of the Universe, the dark matter is said to be decoupled. The evolution of the dark matter number density  $n$ , is governed by the Boltzmann equation [43]:

$$\dot{n} + 3Hn = -\langle\sigma v_{\text{Møller}}\rangle(n^2 - n_{\text{EQ}}^2), \quad (10)$$

where  $H$  is the Hubble constant,  $\sigma v_{\text{Møller}}$  is the total annihilation cross section multiplied by the Møller velocity with  $v_{\text{Møller}} = (|v_1 - v_2|^2 - |v_1 \times v_2|^2)^{1/2}$ , brackets denote thermal average and  $n_{\text{EQ}}$  is the number density in thermal equilibrium. It has been shown that  $\langle\sigma v_{\text{Møller}}\rangle = \langle\sigma v_{\text{lab}}\rangle = 1/2[1 + K_1^2(x)/K_2^2(x)]\langle\sigma v_{\text{cm}}\rangle$  [43], where  $x = m_{\text{DM}}/T$  and  $K_i(x)$  is the modified Bessel functions of the  $i$ -th order. To derive the relic density of the tau flavored dark matter, one needs to calculate the thermal average of the total annihilation cross section. Analytically one can approximate the thermal average  $\langle\sigma v\rangle$  with the non-relativistic expansion  $\langle\sigma v\rangle = a + b\langle v^2\rangle$  in the lab frame,

$$\begin{aligned} \langle\sigma v\rangle &= \sum_{i=1}^4 \zeta_i^2 \left( \frac{m_\psi^2}{32\pi(m_\psi^2 + \hat{m}_i^2)^2} + \langle v^2 \rangle \frac{m_\psi^2(-7m_\psi^4 - 18m_\psi^2\hat{m}_i^2 + \hat{m}_i^4)}{384\pi(m_\psi^2 + \hat{m}_i^2)^4} \right) + \\ &\quad \frac{1}{4}s_{2\theta}^2(\kappa_1^2 - \kappa_2^2)^2 \left( \frac{m_\psi^2}{16\pi(\hat{m}_1^2 + m_\psi^2)(\hat{m}_2^2 + m_\psi^2)} + \frac{\langle v^2 \rangle \Delta}{192\pi(\hat{m}_1^2 + m_\psi^2)^3(\hat{m}_2^2 + m_\psi^2)^3} \right) \\ &\equiv a + b\langle v^2 \rangle, \end{aligned} \quad (11)$$

where

$$\begin{aligned} \Delta &= -m_\psi^2(7m_\psi^8 + 16m_\psi^6(\hat{m}_1^2 + \hat{m}_2^2) + m_\psi^4(5\hat{m}_1^4 + 32\hat{m}_1^2\hat{m}_2^2 + 5\hat{m}_2^4) \\ &\quad + 8m_\psi^2\hat{m}_1^2\hat{m}_2^2(\hat{m}_1^2 + \hat{m}_2^2) - \hat{m}_1^4\hat{m}_2^4). \end{aligned} \quad (12)$$

Here  $\zeta_{1,2}$  were defined below Eq. (8) and  $\zeta_{3,4} = \sqrt{2}\kappa_{1,2}^2$ . The notation  $\hat{m}_i$ , where  $i = 1, 2, 3, 4$ , denotes the mass of  $\hat{\Phi}^+$ ,  $\hat{S}^+$ ,  $\rho$  and  $\eta$  respectively.

The present relic density of the DM is simply given by  $\rho_{\text{DM}} = m_{\text{DM}}n_{\text{DM}} = m_{\text{DM}}s_0Y_\infty$  [31], where  $s_0$  is the present entropy density. The relic abundance can be written in terms of the critical density

$$\Omega h^2 \approx 2 \times \frac{1.07 \times 10^9}{M_{\text{pl}}} \frac{x_F}{\sqrt{g_*}} \frac{1}{a + 3b/x_F}, \quad (13)$$

where  $a$  and  $b$  were defined in Eq. (11),  $M_{\text{pl}}$  is the Planck mass,  $x_F = m_{\text{DM}}/T_F$  with  $T_F$  being the freezing out temperature of the dark matter,  $g_*$  is the degrees of freedom at the

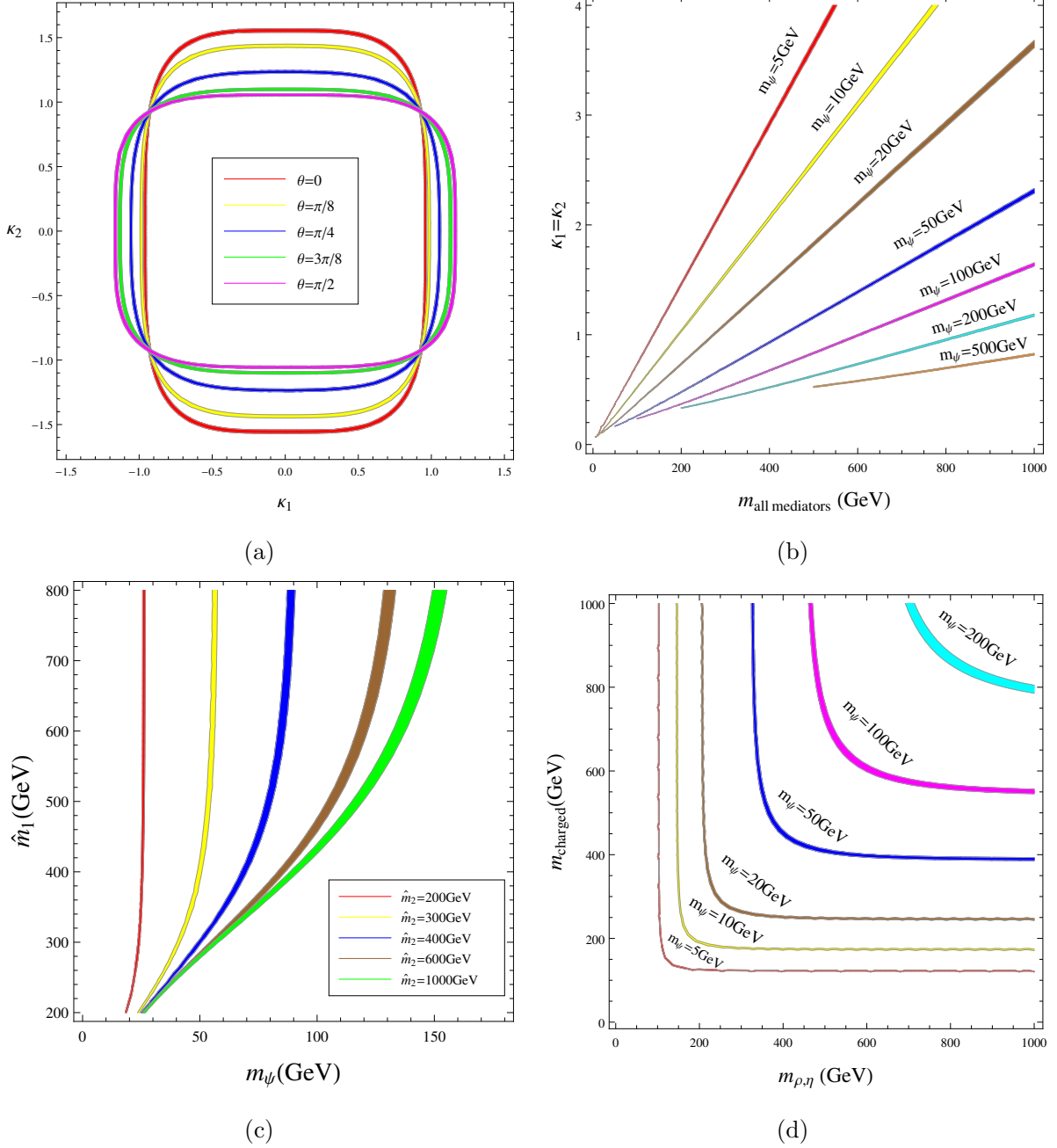


FIG. 3: The contours of the relic density within two standard deviations of the measured value: In Fig. (a), we show contours in  $\kappa_1 - \kappa_2$  plane with different inputs of mixing angle  $\theta$ , by setting  $m_\psi = 100$  GeV,  $\hat{m}_1 = 400$  GeV,  $\hat{m}_2 = 600$  GeV and  $m_\rho = m_\eta = 700$  GeV; In Fig. (b), we show contours in the  $\kappa_1 - m_{\text{all mediators}}$  plane for different dark matter masses, by assuming all mediators have the same mass and  $\kappa_1 = \kappa_2$ ; Fig.(c) show contours in the  $\hat{m}_1 - m_\psi$  plane for different values of  $\hat{m}_2$ , by setting  $\kappa_1 = \kappa_2 = 1$  and  $m_\rho = m_\eta = 700$  GeV; In Fig. (d), we set  $\kappa_1 = \kappa_2 = 1$  and plot charged mediator versus neutral mediator masses for several dark matter masses.



freeze out temperature and the factor 2 on the right-hand side accounts for the fact that dark matter in our model is a Dirac fermion.

The dark matter relic density measured by the Planck experiment is  $\Omega h^2 = 0.1199 \pm 0.0022$  [1]. To check its constraint on the parameter space, we plot in Fig. 3 (a) contours of the dark matter relic density requiring the relic density to be within two standard deviations of the measured central value in the  $\kappa_1 - \kappa_2$  plane by setting  $\hat{m}_1 = 400$  GeV,  $\hat{m}_2 = 600$  GeV and  $m_\rho = m_\eta = 700$  GeV. The red, yellow, blue, green and pink contours correspond to  $\theta = 0, \pi/8, \pi/4, 3\pi/8$  and  $\pi/2$  respectively. One has  $\kappa_{1,2} \in [-1.5, 1.5]$  and  $\kappa_1, \kappa_2$  can not both take small values to give rise to a correct dark matter relic density. By assuming  $\kappa_1 = \kappa_2$  and degenerate mediator masses, we show in Fig. 3 (b) contours of the dark matter relic density, with the red, yellow, brown, blue, magenta, cyan and orange colored contours corresponding to  $m_\psi = 5$  GeV, 10 GeV, 20 GeV, 50 GeV, 100 GeV, 200 GeV and 500 GeV respectively. It shows that the heavier the dark matter is, the larger the annihilation cross section will be, such that larger mediator masses or smaller couplings will be required to get a correct relic density. This can also be seen from Fig. 3 (c) and (d), where we show the correlation between the dark matter mass and the charged mediator masses (Fig. 3 (c)) as well as the correlation between the neutral mediator masses and charged mediator masses (Fig. 3 (d)). For the input of other parameters of Fig. 3 (c) and (d) see the caption for details.

## B. Direct detection

Notice that flavored dark matter models may help to release the tension between the observed dark matter relic density and constraints from direct detections, which detect dark matter scattering from nuclei in underground laboratories. In our model, dark matter couples to nucleons through loop induced electromagnetic form factors of the dark matter as well as loop induced dark matter-Higgs interactions. The effective interactions of the dark matter with nucleon take the following form [21, 30, 32]

$$f_r \bar{\psi} \gamma^\mu \psi \bar{N} \gamma_\mu N + f_h \bar{\psi} \psi \bar{N} N + f_m^1 \bar{\psi} i \sigma^{\mu\nu} \psi \frac{q_\nu}{q^2} \bar{N} K_\mu N + f_m^2 \bar{\psi} i \sigma^{\alpha\mu} \psi \frac{q_\alpha q_\beta}{q^2} \bar{N} i \sigma^{\beta\mu} N \quad (14)$$

with  $q^\mu$  being the momentum transfer from nucleon to dark matter and  $K^\mu$  defined as the summation of momenta of incoming and outgoing nucleon. The Wilson coefficients are given

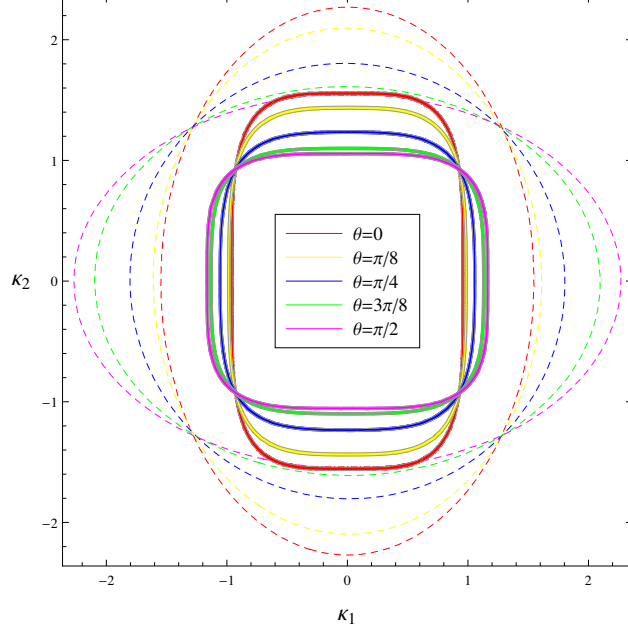


FIG. 4: LUX limit as a dashed line for each solid relic density contour in the  $\kappa_1, \kappa_2$  plane for different  $\theta$ . Relic density contours are within two standard deviations of the Planck measured central value and regions outside the dashed lines are excluded at 95% C.L. by the LUX. The other parameters are fixed to be  $m_\psi = 100$  GeV,  $\hat{m}_1 = 400$  GeV,  $\hat{m}_2 = 600$  GeV,  $m_\rho = m_\eta = 700$  GeV and  $\lambda_2 = \lambda_5 = 0$ .

by

$$f_r^N = eQ_N b_\psi, \quad f_h^N = f_\psi^h \frac{m_N}{m_h^2 v} \left( \sum_{q=u,d,s} f_{T_q}^N + \frac{2}{9} f_{TG}^N \right), \quad f_m^1 = \frac{eQ_N \mu_\psi}{2m_N}, \quad f_m^2 = -\frac{e\tilde{\mu}_N \mu_\psi}{2m_N},$$

where  $Q_N$  is the charge of the nucleon,  $\mu_\psi$  and  $b_\psi$  are the magnetic moment and charge radius of the dark matter respectively,  $\tilde{\mu}_N$  is the nucleon magnetic moment, that is,  $\tilde{\mu}_p \approx 2.80$  and  $\tilde{\mu}_n \approx -1.91$ . Finally  $f_\psi^h$  is the effective dark matter-Higgs coupling,

$$f_\psi^h = \sum_{ij=1}^2 \frac{c_{ij} m_\psi}{32\pi^2} \int_0^1 dx \int_0^{1-x} dy \frac{1-x}{(1-x-y)\hat{m}_i^2 + y\hat{m}_j^2 + (x^2-x)m_\psi^2}, \quad (15)$$

where  $c_{11} \approx \zeta_1 v (\lambda_2 c_\theta^2 + \lambda_5 s_\theta^2 + 2\Lambda s_\theta c_\theta / v)$ ,  $c_{22} \approx \zeta_2 v [\lambda_2 s_\theta^2 + \lambda_5 c_\theta^2 - 2\Lambda s_\theta c_\theta / v]$ ,  $c_{12} = c_{21} = s_\theta c_\theta (\kappa_1^2 - \kappa_2^2) [v s_\theta c_\theta (\lambda_5 - \lambda_2) + \Lambda c_{2\theta}]$  and  $x, y$  are Feynman parameters. We have neglected the  $Z$  mediated interactions in Eq.(14) since they are subdominant compared with photon mediated processes.

The momentum dependence induced by the magnetic moment term makes it impossible to factorize the differential event rate into the product of the elastic cross section and

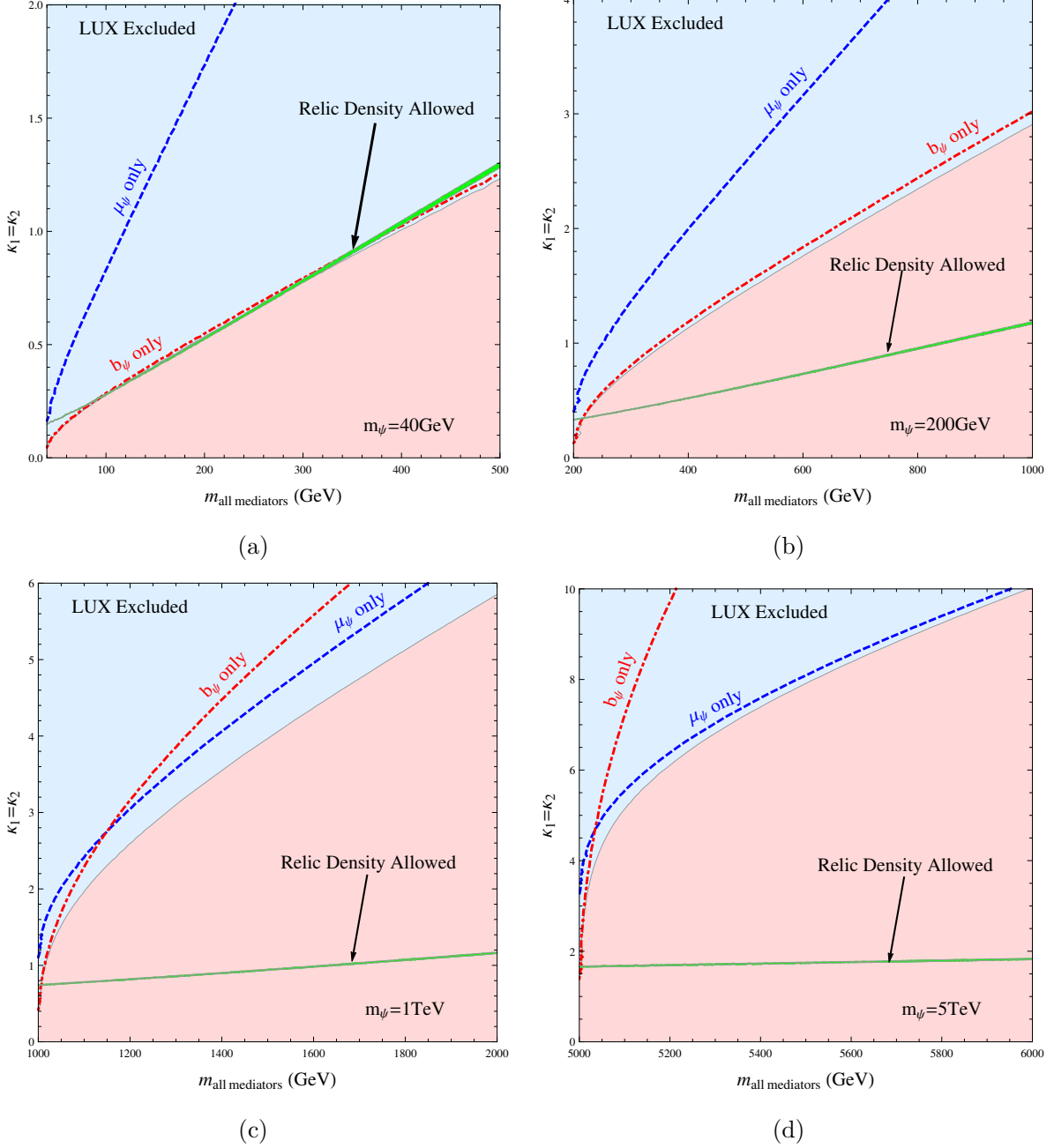


FIG. 5: LUX excluded and relic density allowed regions for dark matter with different masses in the couplings versus mediator mass plane. LUX excluded regions at 95% C.L. are shown in light blue while light red regions are allowed. The “ $\mu_\psi$  only” dashed line is the LUX limit retaining only the contribution of magnetic dipole moment while “ $b_\psi$  only” corresponds to including only charge radius contribution. The green contours are relic density allowed regions within two standard deviations of the Planck central value. In all plots we assume  $\kappa_1 = \kappa_2$ , equal mediator masses and  $\lambda_2 = \lambda_5 = 0$ .

momentum integration. We therefore need to calculate the differential rate numerically then translate the cross section into event rate in experiment. One more complexity arises since the operators shown above go beyond the traditional spin-independent and spin-dependent characterization of dark matter nucleus scattering and therefore more nuclear responses are involved [41]. The corresponding classification of the underlying non-relativistic operators responsible for dark matter nucleon scattering as well as the identification and calculation of nuclear responses for finite-sized nucleus have been performed systematically in an effective field theory framework in Ref. [39, 40] following earlier work in Ref. [38]. This framework has been implemented in the public code [33] together with statistical analysis for each experiment. We therefore use this code in our analysis and refer the reader to the above literatures for details.

We add constraints of the dark matter direct detection to the relic density plot in Fig. 3 (a), and the new plot is shown in Fig. 4. For each relic density contour, we plot its corresponding limit from the LUX [46] at the 95% C. L., which is shown as a dashed line with the same color as the relic density contour. We can see that the LUX allowed maximum magnitude of  $\kappa_{1,2}$  is  $1 \sim 2$  while the corresponding relic density allowed magnitudes are smaller, which are thus allowed by the LUX. Notice that all direct detection limit lines intersect at four points when  $|\kappa_1| = |\kappa_2|$  just like the case of the relic density contours. This is because  $\mu_\psi$  and  $b_\psi$  are both independent on the mixing angle  $\theta$  in this scenario and the contribution arising from the anapole moment is velocity suppressed and thus negligible.

We also show representative plots in Fig. 5 on the correlations between the coupling strength  $\kappa_1 = \kappa_2$  and the totally degenerate mediator masses, where subfigures (a), (b), (c) and (d) correspond to taking the dark matter mass as 40 GeV, 200 GeV, 1 TeV and 5 TeV, respectively. The other parameters are fixed to be  $\lambda_2 = \lambda_5 = 0$ , and  $\Lambda = 0$  as a result of the assumed degenerate charged scalars. So the effective dark matter-Higgs coupling is exactly zero in this scenario. Generally the Higgs mediated contribution is suppressed by the Higgs mass squared and thus subdominant compared with contributions of electromagnetic form factors [42]. In each plot, light blue(red) regions are excluded (allowed) by the LUX at the 95% C. L.; the green contours represent regions where the dark matter relic density is consistent with the measured value within  $2\sigma$  level; the red dot-dashed (blue dashed) line is the LUX limit when considering only the contribution of charge radius (magnetic moment). One can see from these figures the roles played by the magnetic moment and the

charge radius in the dark matter direct detections. For a relatively light dark matter, the charge radius dominates the contribution to the direct detection; while for the superheavy dark matter, the magnetic moment plays more important role. This is because the charge radius operator is dimension six while the magnetic moment operator is dimension five. It also shows that the dark matter should be around 50GeV or heavier to release the tension between the measured dark matter relic density and constraints from the LUX.

### C. Higgs Couplings

Precision measurement of the Higgs couplings is one of the most important tasks in the future Higgs factory. The tau lepton Yukawa coupling was measured by the ATLAS and CMS collaborations, whose results are not so consistent with the SM prediction:  $\mu_{\tau\tau} = 1.4 \pm 0.4$  by the ATLAS collaboration [44] and  $0.78 \pm 0.27$  by the CMS collaboration [45]. In our model, the tau lepton mass arises from two parts: the Yukawa interaction induced term, i.e.,  $m_Y^\tau = y_\tau v / \sqrt{2}$ , as well as loop corrections,  $m_\tau^{\text{loop}}$ , mediated by the dark matter and two charged scalars. The mass can be written as

$$m_\tau \approx y_\tau v / \sqrt{2} + \frac{c_\theta s_\theta \kappa_1 \kappa_2 m_\psi}{16\pi^2} \left[ \frac{\hat{m}_1^2}{\hat{m}_1^2 - m_\psi^2} \ln \left( \frac{\hat{m}_1^2}{m_\psi^2} \right) - \frac{\hat{m}_2^2}{\hat{m}_2^2 - m_\psi^2} \ln \left( \frac{\hat{m}_2^2}{m_\psi^2} \right) \right], \quad (16)$$

where we have neglected terms proportional to  $m_Y^\tau$  in the calculation of  $m_\tau^{\text{loop}}$ . We show in the left panel of Fig. 6 contours of  $m_\tau^{\text{loop}}/m_\tau$  in the  $\hat{m}_1 - \hat{m}_2$  plane by setting  $\kappa_1 = \kappa_2 = 1$ ,  $c_\theta = 0.6$  and  $m_\psi = 100$  GeV which are consistent with dark matter constraints. It is clear that  $m_\tau^{\text{loop}}$  can be  $\mathcal{O}(10\%)$  of the total tau mass.

The branching ratio for the Higgs decaying into  $\tau\bar{\tau}$  can be approximately written as

$$\text{BR}(h \rightarrow \tau\tau) \approx \frac{m_h}{16\pi\Gamma_{\text{tot}}} \left| y_\tau + \sqrt{2}\xi_\tau \right|^2 \quad (17)$$

where  $m_h$  is the SM Higgs mass,  $\Gamma_{\text{tot}} = 4.1 \times 10^{-3}$  GeV is the SM Higgs decay width and the loop induced coupling can be written as

$$\xi_\tau = \sum_{ij=1}^2 \frac{y_{ij} m_\psi}{16\pi^2} \int_0^1 dx \int_0^{1-x} dz \frac{1}{x m_\psi^2 + z \hat{m}_i^2 + (1-x-z) \hat{m}_j^2 - z(1-x-z) m_h^2}, \quad (18)$$

with  $y_{11} = \kappa_1 \kappa_2 c_\theta s_\theta [(\lambda_2 c_\theta^2 + \lambda_5 s_\theta^2) v + \Lambda s_{2\theta}]$ ,  $y_{22} = -\kappa_1 \kappa_2 c_\theta s_\theta [(\lambda_2 s_\theta^2 + \lambda_5 c_\theta^2) v - \Lambda s_{2\theta}]$  and  $y_{12} = y_{21} = 1/2 \kappa_1 \kappa_2 c_{2\theta} [s_\theta c_\theta v (\lambda_5 - \lambda_2) + \Lambda c_{2\theta}]$ . We plot in Fig. 7 the signal rate  $\mu_{\tau\tau}$  associated with Higgs measurements, relative to the SM Higgs expectation, as a function of the dark

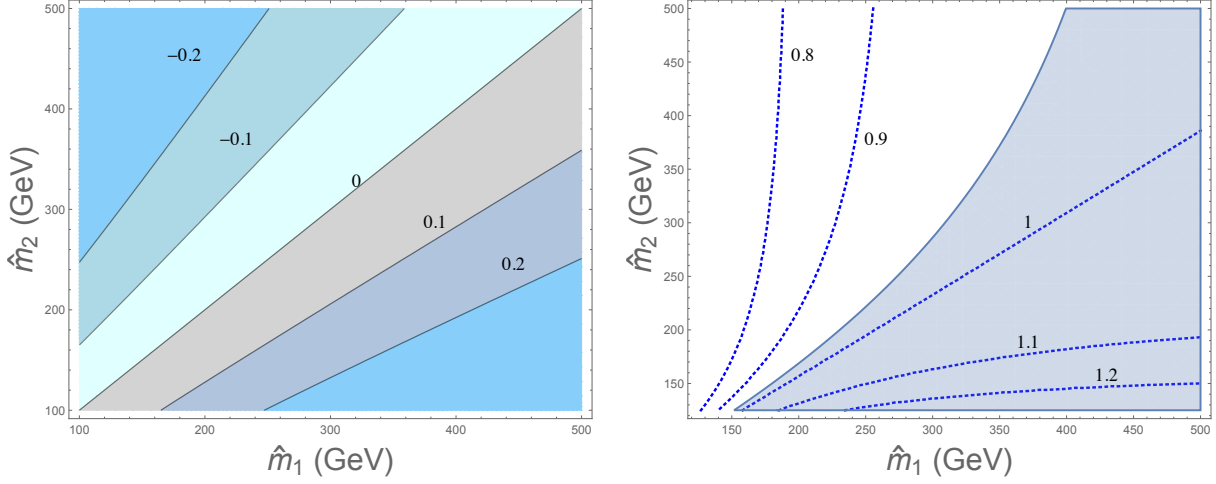


FIG. 6: Left panel: Contours of  $m_\tau^{\text{loop}}/m_\tau$  in the  $\hat{m}_1 - \hat{m}_2$  plane; Right panel: Contours of  $\mu_{\gamma\gamma}$  in the  $\hat{m}_1 - \hat{m}_2$  plane, the cyan color marked region satisfy the combined constraint given by the ATLAS and CMS.

matter mass by setting  $c_\theta = 0.5$ ,  $\lambda_2 = \lambda_5 = 0.1$ ,  $\hat{m}_1 = 400$  GeV and  $\hat{m}_2 = 600$  GeV as well as  $\kappa_1 = -\kappa_2 = 1$  for the red solid curve and  $\kappa_1 = \kappa_2 = 1$  for the blue dashed curve. The dashed and dotted horizontal lines represent central values given by the ATLAS and the CMS respectively with light blue and light yellow bands corresponding to uncertainties at the  $1\sigma$  level. It should be mentioned that  $\mu_{\tau\tau}$  can be significantly changed for some extreme scenarios and the modification can also be tiny for other cases (small  $\kappa_{1,2}$ , light dark matter and heavy degenerate charged scalars).

Due to the existence of charged scalars, the Higgs to diphoton decay width is slightly modified. The decay rate can be written in terms of couplings of the SM Higgs with new charged scalars:

$$\Gamma(h \rightarrow \gamma\gamma) = \frac{G_F \alpha^2 m_h^3}{128 \sqrt{2} \pi^3} \left| -6.48 + \sum_{i=1}^2 \frac{v c_{ii}}{2 \zeta_i \hat{m}_i^2} A_0 \left( \frac{4 \hat{m}_i^2}{m_h^2} \right) \right|^2, \quad (19)$$

where  $-6.48$  is the contribution of the  $W$  and top loops and the second term is the contribution of two new charged scalars with the definition of the loop integral function  $A_0(x)$  following conventions of Ref [34]

$$A_0(x) = -x^2 \left[ \frac{1}{x} - f(x^{-1}) \right] \quad \text{with} \quad f(x) \equiv \begin{cases} \arcsin^2(\sqrt{x}), & \text{for } x > 1, \\ -\frac{1}{4} \left( \ln \frac{1+\sqrt{1-x^{-1}}}{1-\sqrt{1-x^{-1}}} - i\pi \right)^2, & \text{for } x < 1. \end{cases} \quad (20)$$

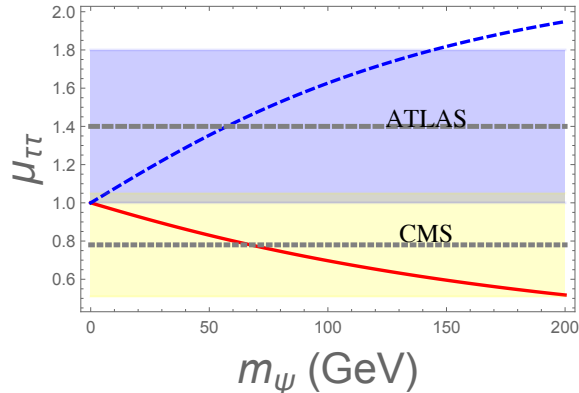


FIG. 7: Signal rate of Higgs to tau tau relative to the SM expectation as a function of the dark matter mass. We set  $c_\theta = 0.5$ ,  $\lambda_2 = \lambda_5 = 0.1$ ,  $\hat{m}_1 = 400$  GeV and  $\hat{m}_2 = 600$  GeV as well as  $\kappa_1 = -\kappa_2 = 1$  for the red solid curve and  $\kappa_1 = \kappa_2 = 1$  for the blue dashed curve.

We plot in the right panel of Fig. 6 contours of  $\mu_{\gamma\gamma}$  in the  $\hat{m}_1 - \hat{m}_2$  plane by setting  $\lambda_2 = \lambda_5 = 0.5$  and  $c_\theta = 0.8$ . The green dashed lines from the left to the right correspond to  $\mu_{\gamma\gamma} = 0.8, 0.9, 1.0, 1.1, 1.2$  respectively. The cyan color marked region satisfies the current combined bound given by the ATLAS and CMS collaborations,  $\mu_{\gamma\gamma} = 1.15 \pm 0.18$ , where  $\mu_{\gamma\gamma} = 1.17 \pm 0.27$  by the ATLAS [36] and  $\mu_{\gamma\gamma} = 1.14^{+0.26}_{-0.23}$  by the CMS [37]. It should be mentioned that the future improved measurements of  $\mu_{\gamma\gamma}$  may put more severe constraint on couplings of the Higgs to new charged scalars.

Finally, let's comment on the collider searches of this model. The collider signals of lepton portal dark matter models are events with charged lepton pairs and missing energy. It was showed in Ref. [7] that these models have clear signals above the SM background in certain parameter space at the LHC. Searches for signatures of our model at the LHC and lepton colliders such as CEPC or ILC, which are interesting but beyond the reach of this paper, will be shown in a future study.

#### IV. CONCLUDING REMARKS

Lepton-flavored dark matter is interesting and appealing for many aspects. In this paper we focused on the phenomenology of the tau-flavored Dirac dark matter model. The electromagnetic form factors of the dark matter which are crucial for the dark matter direct detections, were calculated in the case where there are two types of dark matter - third

generation lepton Yukawa interactions. Our study shows that the tension between the observed dark matter relic density and constraints of dark matter direct detections are highly loosened. The charge radius dominates the contributions to the dark matter direct detection for the light dark matter case, while the magnetic moment plays more important role for heavy dark matter case. In addition the tau Yukawa coupling can be significantly changed in this model, and the one-loop induced tau mass can be  $\mathcal{O}(10\%)$  of the total mass. As a result, the signal rate of  $h \rightarrow \bar{\tau}\tau$ , relative to the SM expectation, measured by the LHC, can be explained in this model. The Higgs to diphoton ratio is also slightly changed but is still consistent with the current LHC constraint.

## ACKNOWLEDGMENTS

The authors are indebted to Prof. Michael J. Ramsey-Musolf for helpful discussions and encouragements. This work was supported in part by DOE Grant de-sc0011095. Huai-Ke Guo was also supported by the China Scholarship Council. We thank Chien Yeah Seng for reading the manuscript.

- 
- [1] P. A. R. Ade *et al.* [Planck Collaboration], arXiv:1502.01589 [astro-ph.CO].
  - [2] S. Chang, R. Edezhath, J. Hutchinson and M. Luty, Phys. Rev. D **90**, no. 1, 015011 (2014) [arXiv:1402.7358 [hep-ph]].
  - [3] Y. Cai and W. Chao, Phys. Lett. B **749**, 458 (2015) [arXiv:1408.6064 [hep-ph]].
  - [4] E. A. Baltz and L. Bergstrom, Phys. Rev. D **67**, 043516 (2003) [hep-ph/0211325].
  - [5] W. Chao, Phys. Lett. B **695**, 157 (2011) [arXiv:1005.1024 [hep-ph]].
  - [6] D. Schmidt, T. Schwetz and T. Toma, Phys. Rev. D **85**, 073009 (2012) [arXiv:1201.0906 [hep-ph]].
  - [7] P. Agrawal, S. Blanchet, Z. Chacko and C. Kilic, Phys. Rev. D **86**, 055002 (2012) [arXiv:1109.3516 [hep-ph]].
  - [8] T. Cohen and K. M. Zurek, Phys. Rev. Lett. **104**, 101301 (2010) [arXiv:0909.2035 [hep-ph]].
  - [9] A. Freitas and S. Westhoff, JHEP **1410**, 116 (2014) [arXiv:1408.1959 [hep-ph]].



- [10] A. DiFranzo, K. I. Nagao, A. Rajaraman and T. M. P. Tait, JHEP **1311**, 014 (2013) [JHEP **1401**, 162 (2014)] [arXiv:1308.2679 [hep-ph]].
- [11] C. Cheung and D. Sanford, JCAP **1402**, 011 (2014) [arXiv:1311.5896 [hep-ph]].
- [12] P. Agrawal, Z. Chacko, C. Kilic and C. B. Verhaaren, JHEP **1508**, 072 (2015) [arXiv:1503.03057 [hep-ph]].
- [13] L. Calibbi, A. Crivellin and B. Zaldvar, Phys. Rev. D **92**, no. 1, 016004 (2015) [arXiv:1501.07268 [hep-ph]].
- [14] C. Kilic, M. D. Klimek and J. H. Yu, Phys. Rev. D **91**, no. 5, 054036 (2015) [arXiv:1501.02202 [hep-ph]].
- [15] C. J. Lee and J. Tandean, JHEP **1504**, 174 (2015) [arXiv:1410.6803 [hep-ph]].
- [16] P. Agrawal, M. Blanke and K. Gemmler, JHEP **1410**, 72 (2014) [arXiv:1405.6709 [hep-ph]].
- [17] P. Agrawal, B. Batell, D. Hooper and T. Lin, Phys. Rev. D **90**, no. 6, 063512 (2014) [arXiv:1404.1373 [hep-ph]].
- [18] B. Batell, T. Lin and L. T. Wang, JHEP **1401**, 075 (2014) [arXiv:1309.4462 [hep-ph]].
- [19] J. Kile, Mod. Phys. Lett. A **28**, 1330031 (2013) [arXiv:1308.0584 [hep-ph]].
- [20] A. Kumar and S. Tulin, Phys. Rev. D **87**, no. 9, 095006 (2013) [arXiv:1303.0332 [hep-ph]].
- [21] S. Chang, R. Edezhath, J. Hutchinson and M. Luty, Phys. Rev. D **90**, no. 1, 015011 (2014) [arXiv:1402.7358 [hep-ph]].
- [22] Y. Bai and J. Berger, JHEP **1408**, 153 (2014) [arXiv:1402.6696 [hep-ph]].
- [23] Y. Bai and J. Berger, JHEP **1311**, 171 (2013) [arXiv:1308.0612 [hep-ph]].
- [24] J. Kile and A. Soni, Phys. Rev. D **84**, 035016 (2011) [arXiv:1104.5239 [hep-ph]].
- [25] Z. H. Yu, X. J. Bi, Q. S. Yan and P. F. Yin, Phys. Rev. D **91**, no. 3, 035008 (2015) [arXiv:1410.3347 [hep-ph]].
- [26] M. C. Chen, J. Huang and V. Takhistov, arXiv:1510.04694 [hep-ph].
- [27] M. Ackermann *et al.* [Fermi-LAT Collaboration], Phys. Rev. Lett. **108**, 011103 (2012) [arXiv:1109.0521 [astro-ph.HE]].
- [28] V. Khachatryan *et al.* [CMS Collaboration], Phys. Lett. B **749**, 337 (2015) [arXiv:1502.07400 [hep-ex]].
- [29] G. Aad *et al.* [ATLAS Collaboration], arXiv:1508.03372 [hep-ex].
- [30] A. Hamze, C. Kilic, J. Koeller, C. Trendafilova and J. H. Yu, Phys. Rev. D **91**, no. 3, 035009 (2015) [arXiv:1410.3030 [hep-ph]].

- [31] G. Bertone, D. Hooper and J. Silk, Phys. Rept. **405**, 279 (2005) [hep-ph/0404175].
- [32] A. and S. Wild, arXiv:1503.03382 [hep-ph].
- [33] M. Cirelli, E. Del Nobile and P. Panci, JCAP **1310**, 019 (2013) [arXiv:1307.5955 [hep-ph]].
- [34] M. Carena, I. Low and C. E. M. Wagner, JHEP **1208**, 060 (2012) [arXiv:1206.1082 [hep-ph]].
- [35] The ATLAS collaboration [ATLAS Collaboration], ATLAS-CONF-2014-061.
- [36] G. Aad *et al.* [ATLAS Collaboration], Phys. Rev. D **90**, no. 11, 112015 (2014) [arXiv:1408.7084 [hep-ex]].
- [37] V. Khachatryan *et al.* [CMS Collaboration], Eur. Phys. J. C **74**, no. 10, 3076 (2014) [arXiv:1407.0558 [hep-ex]].
- [38] J. Fan, M. Reece and L. T. Wang, JCAP **1011**, 042 (2010) [arXiv:1008.1591 [hep-ph]].
- [39] A. L. Fitzpatrick, W. Haxton, E. Katz, N. Lubbers and Y. Xu, JCAP **1302**, 004 (2013) [arXiv:1203.3542 [hep-ph]].
- [40] N. Anand, A. L. Fitzpatrick and W. C. Haxton, Phys. Rev. C **89**, no. 6, 065501 (2014) [arXiv:1308.6288 [hep-ph]].
- [41] M. I. Gresham and K. M. Zurek, Phys. Rev. D **89**, no. 12, 123521 (2014) [arXiv:1401.3739 [hep-ph]].
- [42] A. Ibarra and S. Wild, JCAP **1505**, no. 05, 047 (2015) [arXiv:1503.03382 [hep-ph]].
- [43] P. Gondolo and G. Gelmini, Nucl. Phys. B **360**, 145 (1991).
- [44] G. Aad *et al.* [ATLAS Collaboration], JHEP **1504**, 117 (2015) [arXiv:1501.04943 [hep-ex]].
- [45] S. Chatrchyan *et al.* [CMS Collaboration], JHEP **1405**, 104 (2014) [arXiv:1401.5041 [hep-ex]].
- [46] D. S. Akerib *et al.* [LUX Collaboration], Phys. Rev. Lett. **116**, no. 16, 161301 (2016) doi:10.1103/PhysRevLett.116.161301 [arXiv:1512.03506 [astro-ph.CO]].